Photoelectrochemical Splitting of Water at Nanocrystalline *n*-Fe_2O_3 Thin-Film Electrodes

Shahed U. M. Khan* and Jun Akikusa

Department of Chemistry and Biochemistry, Duquesne University, Pittsburgh, Pennsylvania 15282

Received: January 6, 1999

Semiconducting nanocrystalline thin films of *n*-Fe_2O_3 were synthesized by a spray−pyrolytic method. These films were used for the photoelectrochemical splitting of water to hydrogen and oxygen gases. The rates of photoelectrochemical splitting of water at these thin-film electrodes were found to depend on the spray time, substrate temperature, solvent composition in the spray solution, and the concentration of the spray solution. The maximum photocurrent density of 3.7 mA cm^{-2} at 0.7 V/saturated calomel electrode (SCE) was obtained at the *n*-Fe_2O_3 film synthesized using the optimum condition of substrate temperature of 350 °C, the spray time of 60 s, and the spray solution of 0.11 M $FeCl_3$ in 100% ethanol. The band gap energy of this film was found 2.05 eV. The flatband potential of −0.74 V/SCE and the apparent donor density of 2.2×10^{20} cm^{-3} were found from the Mott−Schottky plots at the AC frequency of 1000 Hz. The *n*-Fe_2O_3 films synthesized using the optimum conditions gave rise to a total conversion efficiency of 4.92% and a practical photoconversion efficiency of 1.84% at an applied potential of 0.2 V/SCE at pH 14.

Introduction

Semiconducting iron oxide (*n*-Fe_2O_3) is suitable to use as a photoelectrode because of its low cost as well as its small band gap energy of ∼2.0 eV, which enables it to absorb most of the photons of solar spectrum. *n*-Fe_2O_3 is naturally abundant in the earth's crust. The photoresponse of *n*-Fe_2O_3 films were investigated by several researchers.[1−8] For example, *n*-Fe_2O_3 films were synthesized by a sputtering method[4] and by pressing powders of Fe_2O_3.[5−7] The *n*-Fe_2O_3 films were also synthesized by the spray pyrolysis method[1,2] on a conducting SnO_2-coated glass substrate. Although the photoresponse of *n*-Fe_2O_3 toward water splitting to hydrogen and oxygen gases was improved by doping with iodine,[2] the optimum reaction conditions of the spray−pyrolytic synthesis of *n*-Fe_2O_3 films have not been investigated.

In this work, we focused on the optimization of spray−pyrolytic synthesis of nanocrystalline *n*-Fe_2O_3 films in terms of spray time, solvent composition in the spray solution, concentration of the spray solution, and the substrate temperature for the efficient photoelectrochemical splitting of water to hydrogen and oxygen gases. Various physical properties, such as quantum efficiency, flatband potential, band gap energy and the doping density, of such nanocrystalline films were also determined.

Experimental Section

Synthesis of *n*-Fe_2O_3 Thin Films by Spray-Pyrolysis Method. An *n*-Fe_2O_3 photoanode was prepared by the spray-pyrolysis method and it was described in detail in earlier reports.[9−12] Conducting, tin-oxide-coated glass sheet (60 Ω cm^2, 1/8 in. thickness Pyrex glass, Swift Glass Company, NY) was used as a substrate for the spray−pyrolytic deposition of nanocrystalline *n*-Fe_2O_3 thin films.

An small area of the tin oxide glass was covered with aluminum foil to prevent the deposition of *n*-Fe_2O_3 films so that this area can be used for the electrical contact. An area of 1.0 cm^2 of tin-oxide-coated glass surface was exposed to the spray solution of $FeCl_3 \cdot 6H_2O$ in ethanol. The concentration of spray solution of $FeCl_3 \cdot 6H_2O$ was varied from 0.08 to 0.14 M and the temperature of the substrate on the hot plate was changed from 310 to 410 °C for the spray−pyrolytic synthesis of *n*-Fe_2O_3 films. The duration of each spray was kept at 10 s, with a 5-min interval to maintain a constant substrate temperature. The electrical contact of these films during photoelectrochemical measurements was made by connecting the uncoated area of the tin oxide surface with an alligator clip connector.

Photoelectrochemical Measurements. The photoelectrochemical measurements were performed in a glass cell with a flat Pyrex glass window to facilitate the transmittance of light to the photelectrode surface. The three-electrode glass cell was used for the photoelectrochemical measurements. The working iron oxide thin film electrode had a surface area of 1.0 cm^2, and a Pt wire and a saturated calomel electrode (SCE) were used as the counter and the reference electrodes, respectively. A constant intensity of 50.0 mW cm^{-2} of light from the Xenon lamp (Kratos model LH 150/1) was maintained, taking into account of the loss through the Pyrex glass window. The intensity of light was measured with a digital radiometer (model IL 1350). A monochromator (Kratos model GM 100) was used to generate the light of a particular wavelength. The electrolyte solution used for the water-splitting reaction was 1.0 M NaOH. A scanning potentiostat (EG & G Princeton Applied Research, model 362) was used for the measurement of photocurrent under an applied potential. The photocurrents (which are the measure of the rate of photoelectrochemical splitting of water) as a function of applied potential were recorded on an X−Y recorder (Houston model RE 0092). A Keithley multimeter was also used to monitor the photocurrent.

AC Impedance Measurements. The AC impedance of *n*-Fe_2O_3 films was measured using an EG & G Two-Phase Lock-In Analyzer (model 5208) equipped with EG & G Potentiostat/Galvanostat (model 273). These instruments were computer controlled by EG & G software (model 378) that automatically adjusted the phase angle during each measurement. The AC amplitude of 10 mV was used for all the measurements. A Pt

10.1021/jp990066k CCC: $18.00 © 1999 American Chemical Society
Published on Web 08/05/1999

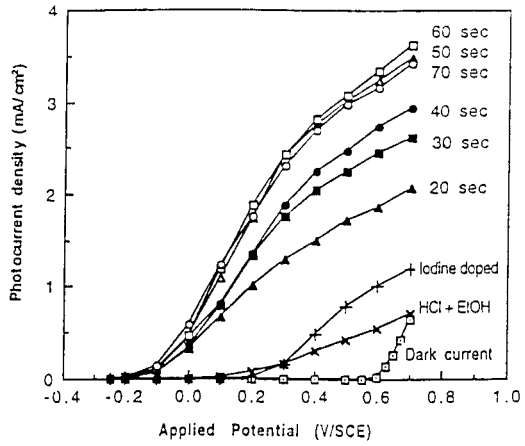

Figure 1. Photocurrent density − applied potential dependence at n-Fe_2O_3 film electrodes synthesized by the spray−pyrolysis method at different spray times, spray solution concentration, 0.11 M $FeCl_3$ in100% EtOH, pyrolysis temperature, 370 °C; light intensity of Xe lamp, 50 mW cm^{-2}, electrolyte solution, 1.0 M NaOH. Previous results[2] at iodine-doped n-Fe_2O_3 films prepared using HCl and EtOH in the spray solution are also included in this figure.

mesh electrode was used as the counter electrode, and the n-Fe_2O_3 films were used as the working electrode. These measurements were carried out in the dark at 1.0 M NaOH solution.

The capacitance, C, was calculated using the following expression of impedance, Z, for a series capacitor−resistor model,

$$Z = Z' + iZ'' \tag{1}$$

where Z' is the real part of the impedance and Z'' is the imaginary part of the impedance. The capacitance C can thus be obtained using

$$Z'' = -i/\omega C \tag{2}$$

with $\omega = 2\pi f$, $i = (-1)^{1/2}$, and f = AC frequency in Hertz. The values of Z'' at different AC frequencies were obtained from Nyquist (Z'' versus Z') plots generated from the measured data of impedance, |Z|, by using EG & G software model 378.

Results and Discussion

Photocurrent Density. *(A) Applied Potential Dependence.* Figure 1 shows the dependence of photocurrent density on the applied potential at spray−pyrolytically synthesized n-Fe_2O_3 films. A highest photocurrent density of 3.7 mA cm^{-2} at 0.7 V/SCE at light intensity of 50 mW cm^{-2} was observed at the n-Fe_2O_3 film synthesized using 60 s spray time at the substrate temperature of 310 °C. Figure 1 also includes the results of photocurrent density at n-Fe_2O_3 synthesized earlier[2] by spray-pyrolysis method including iodine in the spray solution, which consisted of 80% EtOH and 20% of 1.0 M HCl in 0.1 M $FeCl_3$ solution. At the iodine-doped sample[2] maximum photocurrent density of 1.2 mA cm^{-2} (which is 3 times lower than the present result) was observed at the same 0.7 V/SCE and the light intensity of 50 mW cm^{-2}.

It is important to note that the n-Fe_2O_3 films synthesized by the spray−pyrolytic method in the present work gave rise to much higher photocurrent densities compared with those prepared earlier[1,2] using the same method. Furthermore, the n-Fe_2O_3 films synthesized in this work showed higher photoresponse compared to those prepared by compression of n-Fe_2O_3 powder or by thermal oxidation of iron metal sheets.[13−15]

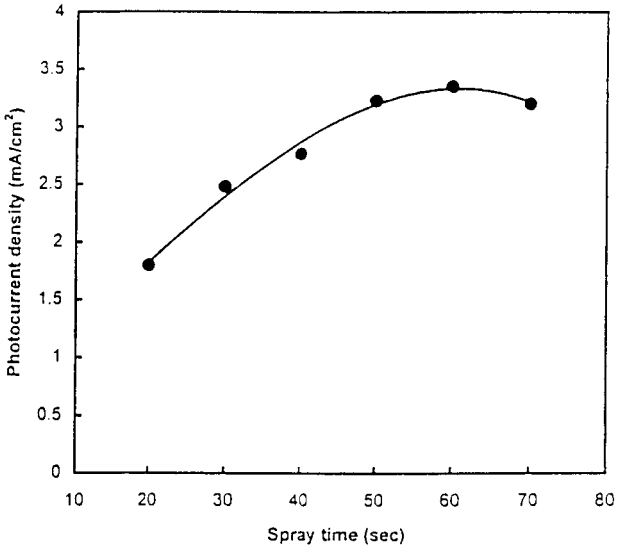

Figure 2. Dependence of photocurrent density on the spray time during spray−pyrolytic synthesis of n-Fe_2O_3 films: spray solution concentration, 0.11 M $FeCl_3$ in 100% ethanol; pyrolysis temperature, 370 °C; applied potential, 0.60 V/SCE; light intensity of Xe lamp, 50 mW cm^{-2}; electrolyte solution, 1.0 M NaOH.

The difference in the results of photocurrent density can be attributed to better quality nanocrystalline film formation under the optimum synthesis conditions used in the present work.

(B) Spray Time Dependence. Figure 2 shows the dependence of photocurrent density on the spray time during spray−pyrolytic deposition of thin films of iron oxide. The increase of photocurrent density with increase of spray time is observed because at higher spray time, the film thickness increases and more light photons can be absorbed at thicker film. However, when the thickness of the film increases further after 60 s of spray time, the photocurrent starts to decrease. This photocurrent decrease can be attributed to the combination of increased resistance and a higher recombination rate of photogenerated carriers due to reduction in the electric field gradient in a thicker film.

The maxima in the plots of photocurrent density versus spray time (see Figure 2) can be better understood from theoretical expressions of photocurrent density.[16−22] A theoretical expression of photocurrent density, j_p, that includes the charge transfer at the photoelectrode−solution interface can be expressed as follows:[22]

$$\begin{aligned} j_p(\text{total}) &= \int j_p(\lambda)\mathrm{d}\lambda \\ &= \int [\{e_0(1-R_\lambda)I_0(\lambda)k_{ct}/(k_{ct}+k_{br}+k_{sr})\}[1- \\ &\quad e^{-\alpha_\lambda W}/\{(1+\alpha_\lambda L_D)(1+G_1(W)L_D{}^{-1})\}- \\ &\quad G_1(W)e^{-\alpha_\lambda W}/\{(L_D+G_1(W)\}]]\mathrm{d}\lambda \end{aligned} \tag{3}$$

with

$$G_1(W) = (\pi kT/4V_{bb}e_0)^{1/2}W \tag{4}$$

where j_p(total) is the integrated photocurrent density, $j_p(\lambda)$ is the wavelength-dependent monochromatic photocurrent density, e_0 is the electronic charge, $I_0(\lambda)$ is intensity of incident light, R_λ is the reflection coefficient, α_λ is the absorption coefficient, W is the width of the space charge region at the interface of the film, L_D is the diffusion length of the photogenerated carriers, V_{bb} is the band bending in the film, and k_{ct}, k_{br}, and k_{sr} represent the three parameters[1]; charge-transfer rate constant at the

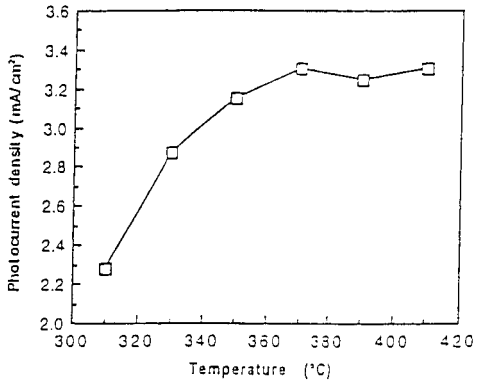

Figure 3. Dependence of photocurrent density on the pyrolysis temperature used for the spray−pyrolytic synthesis of *n*-Fe_2O_3 films: spray solution concentration, 0.11 M $FeCl_3$ in100% EtOH, spray time, 60 s; applied potential, 0.60 V/SCE; light intensity of Xe lamp, 50 mW cm^{-2}; electrolyte solution, 1.0 M NaOH.

interface,[2] bulk recombination rate constant, and surface recombination rate constant of photogenerated carriers,[3] respectively.

Equation 3 indicates that when the recombination is low due to high field drop in the thinner film [i.e., $(k_{br} + k_{sr}) \ll k_{ct}$], the transport of photogenerated carriers in the semiconductor becomes rate limiting. With the increase of the thickness of the film, more light photons are absorbed and consequently photocurrent density increases. However, when the thickness of the film increases further, the field drop reduces to the extent that the recombination of photogenerated carriers (electrons and holes) dominates so that $(k_{br} + k_{sr}) \gg k_{ct}$. This result changes the rate-limiting step to charge transfer at the semiconductor−solution interface. In such films, the increase in k_{br} and k_{sr} decreases the photocurrent and consequently the maxima in Figure 2 results.

Effect of Solvent Composition in the Spray Solution. To enhance the rate of photoelectrochemical splitting of water at nanocrystalline *n*-Fe_2O_3 thin-film electrodes, the solvent composition in the spray solution was varied. A moderate dependence of the photocurrent density on the composition of the solvent was observed, and the highest photocurrent density was found when the solvent in the spray solution was 100% EtOH. This result indicates that the 100% ethanol solvent helps to generate better quality nanocrystals during spray−pyrolytic synthesis because ethanol has much higher heat of combustion (326.68 kJ mol^{-1}) compared to that of methanol (173.64 kJ mol^{-1}). We also observed that the addition of 20% 1.0 M HCl acid in the spray solution decreased the photoresponse to a considerable extent.

The Effect of Substrate Temperature. The dependence of photocurrent density on substrate temperature during the spray−pyrolytic deposition of *n*-Fe_2O_3 thin film is shown in Figure 3. The photocurrent density becomes limiting when the substrate temperature is ∼370 °C. Also, with the decrease of substrate temperature, the photoresponse of *n*-Fe_2O_3 decreases remarkably. We speculate that at low substrate temperature, the pyrolysis was not complete and as a result the quality of the nanocrystals became poor by producing dislocations and kink sites. These dislocations and kink sites act as the recombination centers for the photogenerated electron−hole pairs and consequently the photocurrent density decreases (see eq 3).

Reproducibility of Spray−Pyrolytic Synthesis of n-Fe_2O_3 Thin Films. It is important to test the reproducibility of the synthesis of *n*-Fe_2O_3 thin films by the spray−pyrolysis method. The reproducibility was tested for the *n*-Fe_2O_3 films synthesized

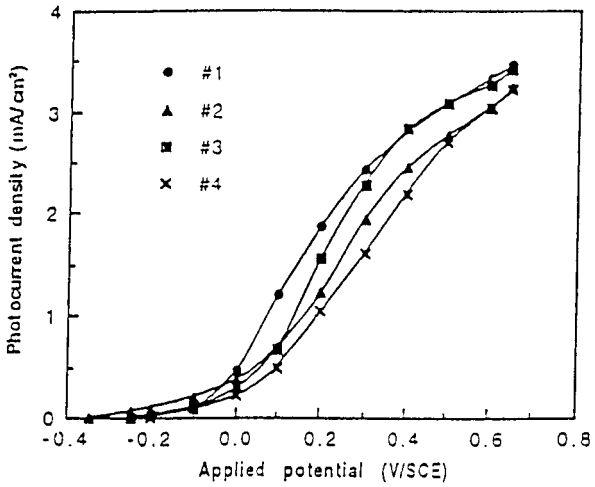

Figure 4. Reproducibility test of the spray−pyrolytic synthesis of *n*-Fe_2O_3 films. The photocurrent density − applied potential dependence of four *n*-Fe_2O_3 films synthesized by spray−pyrolysis method: spray solution concentration, 0.11 M $FeCl_3$ in 100% EtOH; spray time, 60 s; pyrolysis temperature, 370 °C; light intensity of Xe lamp, 50 mW cm^{-2}; electrolyte solution, 1.0 M NaOH.

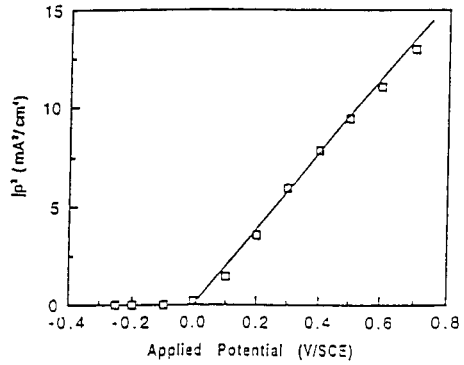

Figure 5. Onset potential determination from j_p^2 − applied potential dependence for *n*-Fe_2O_3 films: spray solution concentration, 0.11 M $FeCl_3$ in 100% EtOH; spray time, 60 s; pyrolysis temperature, 370 °C; light intensity of Xe lamp, 50 mW cm^{-2}; electrolyte solution, 1.0 M NaOH.

at optimum substrate temperature of 370 °C for 60 s using the spray solution of 0.11 M $FeCl_3$ in 100% ethanol.

Figure 4 shows the photocurrent, j_p − potential (E), dependence of several *n*-Fe_2O_3 films prepared at the optimum synthesis condition already mentioned. The open circuit potential did not change and stayed at −0.45 V/SCE ± 0.03 V. The magnitude of the photocurrent density was affected especially at the middle of the S-curve and less affected near 0.60 V/SCE. An average photocurrent density of 3.06 mA cm^{-2} (3.0, 3.0, 3.1, 3.15 mA cm^{-2}) was found at 0.6 V/SCE for these samples. These data correspond to a standard deviation (σ) of 0.065 mA cm^{-2}, which indicates a good reproducibility of the spray−pyrolytically synthesized *n*-Fe_2O_3 films in this work.

Onset Potential from j_p^2 − Potential (E) Plots. Figure 5 shows j_p^2 − potential (E) dependence of *n*-Fe_2O_3 films. A straight line was observed with an intercept at 0.0 V/SCE. This potential of 0.0 V/SCE represents the onset potential for the generation of photocurrent density in the milliamperes range in 1.0 M NaOH solution of pH 14.

Quantum Efficiency. The quantum efficiency under monochromatic light illumination, $\eta(\lambda)$, was calculated using the following relation:[23]

$$\eta(\lambda) = j_p(\lambda)/e_o I_o(\lambda) \quad (5)$$

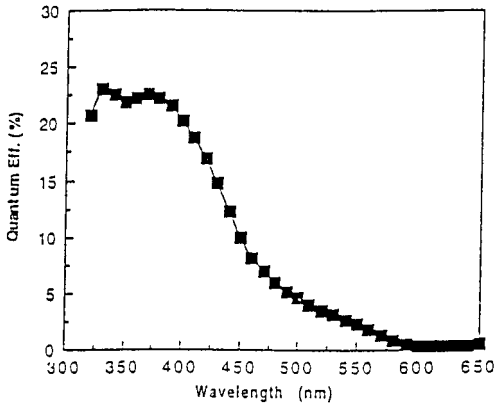

Figure 6. Quantum efficiency, η, versus wavelength for n-Fe_2O_3 films synthesized at 370 °C: spray solution concentration, 0.11 M $FeCl_3$ in 100% EtOH, spray time, 60 s; applied potential, 0.60 V/SCE; electrolyte solution, 1.0 M NaOH.

where j_p (λ) is the monochromatic photocurrent density, e_o is electronic charge, and I_o (λ) is the flux of incident photon at wavelength λ.

The quantum efficiency of n-Fe_2O_3 films was calculated using eq 5, and the results are shown in Figure 6. The quantum efficiency starts to increase near 600 nm, with energy of 2.07 eV. The maximum quantum efficiency of 22.5% was obtained at 370 nm. This value of low quantum efficiency indicates higher recombination of photogenerated holes in the n-Fe_2O_3 film prior to reaction with the OH^- in the electrolyte solution.

Band Gap Energy. The band gap energy, E_g of semiconducting TiO_2 films can be determined using the following equation:[24,25]

$$\eta(\lambda)h\nu = A(h\nu - E_g)^n \qquad (6)$$

where A is a constant, and n equals either 0.5 for allowed direct transition or 2 for allowed indirect transitions. The allowed direct transition of an electron from the valence band to the conduction band by light energy, $h\nu$, is not phonon assisted because such a transition does not need any change in momentum (momentum is conserved). For the indirect band gap, the transition of an electron is phonon assisted because such a transition involves change in both energy and momentum. In the case of the indirect transition, momentum is conserved via a phonon interaction because light photons cannot provide a change in momentum.[25] Furthermore, eq 6 is most appropriate to use when the applied potential is far from the flatband potential, so that the transport of photogenerated carriers inside the semiconductor becomes the rate-determining step.[26]

The band gap energy of n-Fe_2O_3 film was determined using eq 6. Figure 7 shows the plot of $(\eta h\nu)^{1/2}$ versus $h\nu$. A straight line was observed and an intercept was obtained at 2.05 eV that corresponds to the band gap energy of the n-Fe_2O_3 film. Several values of optically measured band gap energy of n-Fe_2O_3 were reported, such as 2.3 eV[1] and 1.97 eV[2]. The band gap energy of 2.05 eV is close to earlier reported value of 2.10 eV, which was determined from the constants of ionization energy and the electron affinity.[27]

Flatband Potential from Mott−Schottky Plots. It is well-known that the flatband potential (E_{fb}) of a semiconductor can be obtained from the intercept of Mott−Schottky plot using the following relation:

$$1/C^2 = (2/e_o\epsilon\epsilon_o N_d)(E_{app} - E_{fb} - kT/e_o) \qquad (7)$$

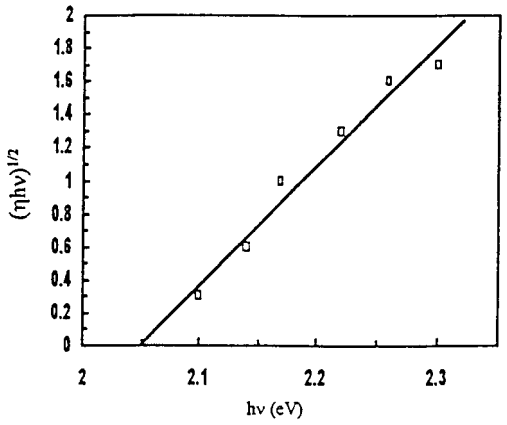

Figure 7. Band gap determination of n-Fe_2O_3 film from the $(\eta h\nu)^{1/2}$ versus $h\nu$ plot: spray solution concentration, 0.11 M $FeCl_3$ in 100% EtOH; spray time, 60 s; pyrolysis temperature, 370 °C; applied potential, 0.60 V/SCE; light intensity, 50 mW cm^{-2}; electrolyte solution, 1.0 M NaOH.

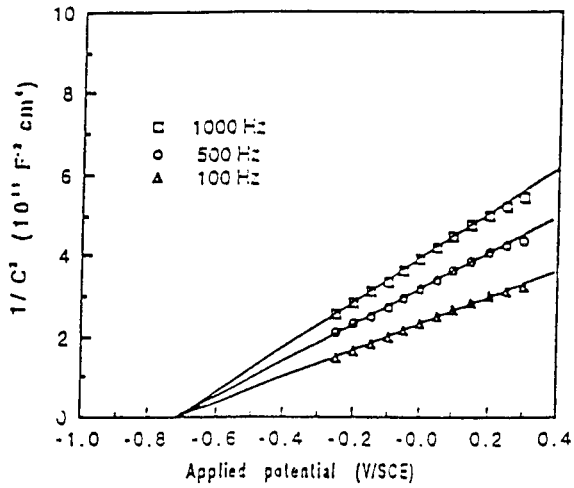

Figure 8. Mott−Schottky ($1/C^2$ versus applied potential, where C is the capacitance) plot for n-Fe_2O_3 films measured at various AC frequencies in the dark condition: electrolyte solution, 1.0 M NaOH; AC amplitude, 10 mV; dielectric constant of Fe_2O_3, 12; spray solution concentration, 0.11 M $FeCl_3$ in 100% EtOH, spray time, 60 s; pyrolysis temperature, 370 °C.

where ϵ is the dielectric constant of the semiconductor, ϵ_o is the permittivity of the vacuum, N_d is the donor density, E_{app} is the applied potential, and kT/e_o is the temperature-dependent term in the Mott−Schottky equation.

Figure 8 shows the Mott−Schottky plot for the n-Fe_2O_3 film at various AC frequencies in the electrolyte solution of 1.0 M NaOH in the dark. In Figure 8, straight lines are observed at all the AC frequencies used for the measurement of impedance.

For n-Fe_2O_3 film, a single intercept was obtained at −0.71 V/SCE for the AC frequencies between 100 and 1000 Hz, giving a flatband potential of −0.74 V/SCE at pH 14 that included the kT/e_o term.

Effect of pH of the Electrolyte Solution on Flatband Potential. Figure 9 shows the Mott−Schottky plots for the n-Fe_2O_3 films in two electrolyte solutions, one having pH = 0 (0.5 M H_2SO_4) and another having pH = 14 (1.0 M NaOH). The AC frequency of 1000 Hz was used for the measurement of impedance. A parallel shift of the plot toward positive potential was observed without any change in the slopes when the pH was changed from 14.0 to 0.0. The intercept of the lines in 0.5 M H_2SO_4 and 1 M NaOH were at 0.18 and − 0.70 V/SCE, respectively. This potential shift (ΔE) of −0.88 V is

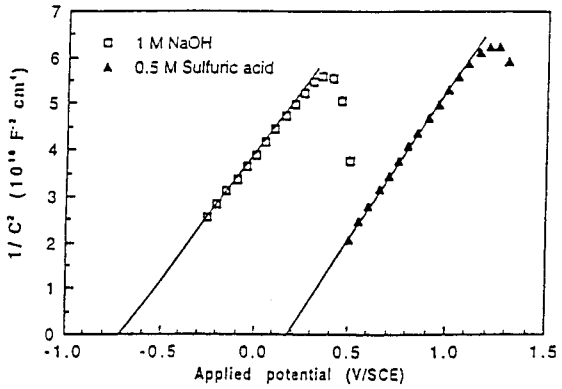

Figure 9. Dependence of Mott−Schottky plot on pH of the solution for *n*-Fe_2O_3 films measured at AC frequency of 1000 Hz, AC amplitude of 10 mV, spray solution concentration of 0.11 M $FeCl_3$ in 100% EtOH, spray time of 60 s, and pyrolysis temperature of 370 °C.

consistent with the change of potential by −0.06 V/pH.

Donor Density in *n*-Fe_2O_3 Films. The donor density in *n*-Fe_2O_3 films was determined from the slope of the Mott−Schottky plot in Figure 8. The dielectric constant of *n*-Fe_2O_3 film used was 12.[28] Because the slopes of these plots changed with the AC frequency, the donor density also changed due to inclusion of varying concentration of surface states at different frequencies.[29−33] Such donor density can be termed as the apparent donor density because donor density itself should not depend on AC frequency. Donor density is generally determined by separating the frequency-dependent contribution of the surface state capacitance by identifying the appropriate equivalent circuit using the detail lumped parameter complex plane analysis.[29−31]

The AC frequency dependence of the apparent donor density of *n*-Fe_2O_3 was relatively small, giving donor densities of 2.2 × 10^{20}, 2.7 × 10^{20}, and 3.6 × 10^{20} cm^{-3} at the AC frequencies of 1000, 500, and 100 Hz, respectively. The increase in the apparent donor density with the decrease of AC frequency can be attributed to the fact that at lower frequency, some contribution may come from the surface states.[29−33]

The apparent donor density at the AC frequency of 1000 Hz was 2.2 × 10^{20} cm^{-3}. For comparison, the apparent donor density of *n*-Fe_2O_3 prepared by the compression of Fe_2O_3 powder with subsequent sintering was reported earlier as 7.0 × 10^{19} cm^{-3}, measured at the same AC frequency of 1000 Hz.[34] The higher donor density of the pyrolytically synthesized *n*-Fe_2O_3 films in this work may be responsible for higher photocurrent density because they reduced the resistivity of the films.

Conversion Efficiency. The total conversion efficiency (light and electrical energy) of the cell, ϵ_{eff} (total), to chemical energy in the presence of an external applied potential under illumination can be given with some modification of an earlier expression[1,35,36] as follows:

$$\% \epsilon_{eff} \text{ (total)} = [(\text{total power output})/(\text{light power input})] \times 100$$

$$= [(j_p E^o_{rev})/(I_o)] \times 100 \quad (8)$$

where the total power output is $j_p E^o_{rev}$; the power input from the light source is I_o, the light intensity is in mW cm^{-2}, j_p is the photocurrent density, which corresponds to the rate of photoassisted water-splitting reaction, E^o_{rev} is the standard reversible potential, which is 1.23 V/NHE for the water-splitting reaction at pH = 0.0. Using I_o = 50 mW cm^{-2} and j_p = 2.0 mA cm^{-2} at E_{app} = 0.2 V/SCE at pH = 14 (which is equal to1.27 V/NHE at pH = 0) in eq 8, the total conversion efficiency was found to be 4.92%.

However, the practical photoconversion efficiency, $\epsilon_{eff, photo}$ (practical), of light energy to chemical energy in the presence of an applied potential, E_{app}, can be written with some modification of earlier expression[1,35,36] as follows:[37]

$$\% \epsilon_{eff, photo} \text{ (practical)} = [(\text{total power output} - \text{electrical power input})/(\text{light power input})] \times 100$$

$$= [j_p(E_{onset} - E_{app})/I_o] \times 100 \quad (9)$$

where $E_{onset} = E^o_{rev}$ for the ideal situation when reaction occurs at thermodynamic standard reversible potential, E^o_{rev}. However, $E_{onset} = (E^o_{rev} + E_{overvoltage})$ is the practical onset potential at which the reaction to split water actually occurred. This potential includes the overvoltage, $E_{overvoltage}$, for the water-splitting reaction, and the photoelectrochemical system had to supply this potential to split water at the observed rate j_p, which would be higher in the absence of overvoltage. Note that we did not include the contribution of electrical power, $j_p E_{app}$, as input power because we used the photocurrent density instead of total illumination current density in eqs 8 and 9.

Using I_o = 50 mW cm^{-2}, j_p = 2.0 mA cm^{-2} at an applied potential, E_{app} = 0.2 V/SCE at pH 14 (= 1.27 V/NHE at pH 0.0), and E_{onset} = 1.73 V/NHE (for a minimum $E_{overvoltage}$ = 0.5 V/NHE) in eq 9, the practical conversion efficiency was found to be 1.84%.

Note that if the minimum overvoltage were not included in eq 9, a negative photoconversion efficiency (−0.16%) would be obtained, which is unrealistic as evident when photocurrent was observed experimentally under illumination. The observed photocurrent represents the conversion of photon energy to chemical energy. Consequently, photoconversion efficiency should not be negative when the photocurrent is observed.

In conclusion, it should be pointed out that spray−pyrolytically synthesized nanocrystalline iron oxide thin films of optimum thickness, crystal structure, and doping density can serve as an inexpensive photoanode for an efficient photoelectrochemical water-splitting reaction.

Acknowledgment. We gratefully acknowledge the partial support of this work by ALCOA Foundation.

References and Notes

(1) Majumder, S. A.; Khan, S. U. M. *Int. J. Hydrogen Energy* **1994**, *19*, 881.
(2) Khan, S. U. M.; Zhou, Z. Y. *J. Electroanal. Chem.* **1993**, *357*, 407.
(3) Battaglia, V.; Newman, J. *J. Electrochem. Soc.* **1995**, *142*, 1423.
(4) Virtanen, S.; Schmuki, P.; Böhni, H.; Vuoristo, P.; Mäntylä, T. *J. Electrochem. Soc.* **1995**, *142*, 3067.
(5) Schmuki, P.; Büchler, M.; Virtanen, S.; Böhni, H.; Muller, R.; Gauckler, L. J. *J. Electrochem. Soc.* **1995**, *142*, 3336.
(6) McGregor, K. G.; Calvin, M.; Otvos, J. W. *J. Appl. Phys.* **1979**, *50*, 369.
(7) Khader, M. M.; Lichtin, N. N.; Vurens, G. H.; Salmeron, M.; Somorjai, G. A. *Langmuir* **1987**, *3*, 303.
(8) McAlpine, N. S.; Fredlein, R. A. *J. Electroanal. Chem.* **1989**, *272*, 101.
(9) Chopra, K. L.; Kainthla, R. C.; Pandya, D. K.; Thakoor, A. P. *Physics of Thin Films* **1982**, *12*, 165.
(10) Shanthi, E.; Banerjee, A.; Chopra, K. L. *Thin Solid Films* **1982**, *88*, 93.
(11) Shanthi, E.; Dutta, V.; Banerjee, A.; Chopra, K. L. *J. Appl. Phys.* **1981**, *51*, 6243.
(12) Kane, J.; Schweizer, H. P.; Kern, W. *J. Electrochem. Soc.* **1976**, *123*, 270.
(13) Leygraf, C.; Hendewerk, M.; Somorjai, G. A. *J. Phys. Chem.* **1982**, *86*, 4484.

(14) Kennedy, J. H.; Anderman, M. *J. Electrochem. Soc.* **1983**, *131*, 848.
(15) Kennedy, J. H.; Frese, K. W., Jr. *J. Electrochem. Soc.* **1978**, *125*, 709.
(16) Wilson, R. *J. Appl. Phys.* **1977**, *48*, 4297.
(17) Butler, M. A. *J. Appl. Phys. Lett.* **1977**, *49*, 1941.
(18) Reiss, H. *J. Electrochem. Soc.* **1978**, *125*, 937.
(19) Reichmann, J. *Appl. Phys. Lett.* **1981**, *35*, 251.
(20) Khan, S. U. M.; Bockris, J. O'M. *J. Appl. Phys.* **1981**, *52*, 270.
(21) Itoh, K.; Bockris, J. O'M. *J. Appl. Phys.* **1984**, *56*, 874; *J. Electrochem. Soc.* **1984**, *131*, 1266.
(22) Khan, S. U. M.; Bockris, J. O'M. *J. Phys. Chem.* **1984**, *88*, 2504.
(23) Bockris, J. O'M.; Szklarczyk, M.; Contractor, A. Q.; Khan, S. U. M. *Int. J. Hydrogen Energy* **1984**, *9*, 741.
(24) Searrson, P. C.; Latanision, R. M. *J. Electrochem. Soc.* **1988**, *135*, 1358.
(25) Pankove, J. I. *Optical Processes in Semiconductor*; Dover: New York, 1971; Chapter 3.
(26) Bockris, J. O'M.; Khan, S. U. M. *Surface Electrochemistry*; Plenum: New York, 1993; Chapter 5.
(27) Samsonov, G. V. *The Oxide Handbook*; IFI/Plenum Data: New York, 1978.
(28) *Handbook of Chemistry and Physics*, 74th ed.; Lide, D. R., ed.; CRC: Boca Raton, FL, 1994.
(29) Alim, M. A. *J. Appl. Phys.* **1995**, *78*, 4476.
(30) Alim, M. A.; Seitz, A. A.; Hirthe, R. *J. Appl. Phys.* **1988**, *63*, 2337.
(31) Morris, G. *J. Vac. Sci. Technol.* **1976**, *13*, 926.
(32) Popescu, V.; Maracione, L.; Spataru, N. *Rev. Roum. Chem.* **1994**, *39*, 769.
(33) Seitz, M. A. *Int. J. Hybr. Microelec.* **1980**, *3*, 1.
(34) Kennedy, J. H.; Frese, K. W., Jr. *J. Electrochem. Soc.* **1978**, *125*, 723.
(35) Bockris, J. O'M.; Murphy, O. J. *Appl. Phys. Comm.* **1983**, *2*, 203.
(36) Khan, S. U. M.; Majumder, S. A. *Int. J. Hydrogen Energy* **1989**, *14*, 653.
(37) Note that when instead of photocurrent density the illumination (photo + dark) current density, j_{ill}, is used, the practical photoconversion efficiency can be expressed as $\% \epsilon_{eff,\ photo}$ (practical) $= [j_{ill}(E_{onset} - E_{app})/(I_o + j_{ill}E_{app})] \times 100$.